Mon. Not. R. Astron. Soc. **000**, 1–10 () Printed 3 March 2024 (MN LATEX style file v2.2)

Morpho-kinematics of the planetary nebula NGC 3242: an analysis beyond its multiple-shell structure⋆

M. A. Gómez-Muñoz[1]†, M. W. Blanco Cárdenas[1], R. Vázquez[1], S. Zavala[2,3], P. F. Guillén[1] and S. Ayala[4]

[1]*Instituto de Astronomía, Universidad Nacional Autónoma de México, Apdo. Postal 877, 22800 Ensenada, B. C., Mexico*
[2]*Instituto Tecnológico de Ensenada, Blvd. Tecnológico No. 150, 22780 Ensenada, B. C., Mexico*
[3]*Instituto de Estudios Avanzados de Baja California, A. C., Blvd. Tte. Azueta 147, Edif. Matematikè Planta Baja, 22800 Ensenada, B. C., Mexico*
[4]*Facultad de Ciencias Físico-Matemáticas, Universidad Autónoma de Nuevo León, Av. Universidad s/n, 66451 San Nicolás de los Garza, N. L., Mexico*

Accepted 2015 August 18. Received 2015 August 17; in original form 2015 May 4

ABSTRACT

In this paper we present the results of optical high-resolution imaging and spectroscopy of the complex planetary nebula (PN) NGC 3242. Our study is based on the analysis of the narrowband Hα λ6563Å, [O III] λ5007Å, [N II] λ6584Å, and [S II] λ6724Å images, and high-resolution spectroscopy using spectral ranges centered on the Hα λ6564Å, [N II] λ6583Å, and [O III] λ5007Å. We detected and analysed morphological components beyond the multiple shell structure of this PN, to investigate the small-scale morphological components aligned towards its major axis (such as knots and ansae, as well as the arc-like features) and its surroundings. Thus, we investigated the morpho-kinematical properties of NGC 3242, as well as their nature and formation. Our results regarding the elliptical double-shell structure and the distance to this nebula are in concordance with previous studies. Furthermore, we have used the software SHAPE to construct a 3D model of NGC 3242, allowing us to successfully reproduce our observational data. We conclude that the prominent knots emitting in the [N II] line are fast, low-ionisation emission regions (FLIERs) related to high velocity jets and the so-called ansae-like features rather resemble bubbles. The disruptions immersed in the halo, whose emission was detected in the the [O III] high-excitation emission line, remarkably display high velocities and were formed likely in an earlier ejection event, in comparison to the innermost FLIERs and bubbles. Finally, according to our model, the kinematical ages of the structures in NGC 3242 range from 390 to 5400 yr.

Key words: ISM: jets and outflows – ISM: kinematics and dynamics – planetary nebulae: individual: NGC 3242

1 INTRODUCTION

Planetary Nebulae (PNe) evolve from low and intermediate-mass stars (0.8 – 8 $M_\odot$) and mainly consist of an ionised gaseous envelope surrounding a stellar nucleus. The shaping of a PN takes place at some point between the asymptotic giant branch (AGB) and the white dwarf stellar phases. The characteristic ionised envelope of a PN results from the strong mass-loss experienced during the AGB and post-AGB phases through the stellar wind ejected by their progenitor stars. The interacting stellar wind model (ISW, Kwok, Purton & Fitzgerald 1978) and its generalisation (GISW, Balick 1987) provide a good explanation to the shaping of the spherical, elliptical, and even slightly bipolar morphologies. However, the formation of more complex morphologies often displaying collimated outflows, high velocity jets, and point symmetric features remains under debate (see Balick & Frank 2002, for a review).

Beyond the ionised envelope and the morphological structures therein, huge haloes have been found in several evolved PNe, giving them a triple-shelled structure. These haloes are ionised by D-type fronts and are the remnant of the AGB envelope (Steffen & Schönberner 2003). Furthermore, imaging using the Hubble Space Telescope (*HST*) have revealed the presence of features resembling rings and arcs immersed in the haloes of four PNe: Hb 5, NGC 6543, NGC 7027 (Terzian 1997) and NGC 3918 (Corradi et al. 2003). As for ground-based imaging, Corradi et al. (2004) have exposed the presence of these arc-like features in NGC 40 and NGC 3242 using the 2.5-m Isaac Newton Telescope

⋆ Based upon observations acquired at the Observatorio Astronómico Nacional in the Sierra San Pedro Mártir (OAN-SPM), Baja California, Mexico.
† E-mail:marcog@astro.unam.mx

(INT). These rings and arc-like structures in the haloes likely arise at the end of the AGB phase, during the last 10,000 to 20,000 years, however, according to Corradi et al. (2004), this phenomenon is not related with the thermal pulses.

NGC 3242 (a.k.a. 'The Ghost of Jupiter') is a multiple-shell PN. The brightest inner ellipse (hereafter referred as inner shell) has a size of 28×20 arcsec and, according to Balick (1987), is expanding at ≃30 km s^{-1} and has a density of 2,200 cm^{-3} (Ruiz et al. 2006). This inner shell is surrounded by an expanding, fainter, moderately elliptical shell (hereafter referred to outer shell) of 46×40 arcsec in size whose density declines $\propto r^{-1/2}$ (Ruiz et al. 2011). Between the inner shell and the outer shell of NGC 3242, the presence of a bright pair of knots detected in [N II] and two ansae-like structures orientated towards NW-SE is remarkable (Balick et al. 1998). The observations of Ruiz et al. (2011) using XMM-Newton have shown the X-ray luminosity is $\simeq 2\times10^{30}$ erg s^{-1} for a distance of 0.5 kpc (Terzian 1997). The electronic temperature of the hot bubble region, in which the X-rays are produced, has a value of $\simeq 2.35\times10^{6}$ K.

These two shells are enclosed by a broken halo revealed by deep images (Corradi et al. 2003, 2004) and at least three rings and two arc-like features are observed within this halo. Monreal-Ibero et al. (2005) have found an apparent gradient in the electronic temperature of the halo increasing towards its outer regions (15,700 K< T_e <20,300 K). Blanco Cárdenas (2006) and Phillips et al. (2009) also noted some arc-like features in the halo, disrupting the rings. Given the location and orientation of these features, they are probably associated with the bright [N II] knots and ansae-like structures observed between the inner shell and the outer shell.

NGC 3242 also shows an outermost huge halo detected by means of *Spitzer* imaging (Ramos-Larios & Phillips 2009). The characteristics of this asymmetric halo, composed by gas and thermal dust grains, extending towards the north, suggest an interaction of NGC 3242 with the ISM. Despite the kinematics of NGC 3242 has been studied before (Balick 1987; Meaburn, López, & Noriega-Crespo 2000; Rodríguez et al. 2010), in this paper we pursue a detailed analysis of the small-scaled structures detected along the major axis, distributed in the multiple-shell structure of this PN, focusing our attention in the puzzling arc-like features in the halo.

2 OBSERVATIONS

2.1 CCD direct images

Narrow-band CCD direct images of NGC 3242 were obtained on 2004 May 9 and 10 using the 1.5-m ($f/13$) Harold Johnson Telescope at the San Pedro Mártir Observatory (OAN-SPM[1]). The detector was a 1024×1024 SITe CCD (24 μm pixel size) with a plate scale of 0.25 arcsec pix^{-1}. The filters used to acquire the images were Hα ($\lambda_c = 6563$Å, $\Delta\lambda = 10$Å), [O III] ($\lambda_c = 5007$Å, $\Delta\lambda = 50$Å), [N II] ($\lambda_c = 6584$Å, $\Delta\lambda = 11$Å), and [S II] ($\lambda_c = 6724$Å, $\Delta\lambda = 10$Å). Exposure times were 180 s for [O III] and 600 s for the other filters. Seeing was around 2-arcsec during observations. Images were processed using standard techniques of the image reduction and analysis facility package (IRAF). Figure 1 shows all the images. Labels are explained in Sect. 3.

2.2 Long-slit echelle spectroscopy

High-resolution, long-slit spectra of NGC 3242 were obtained on different observing runs. Observations were carried out with the Manchester Echelle Spectrograph (MES; Meaburn et al. 2003) in the 2.1-m ($f/7.5$) telescope at OAN-SPM. A e2v 13.5-μm pix^{-1} CCD with 2048×2048 pixels was used as detector. The slit width was 150 μm (1.9 arcsec). Slits positions are shown in Figure 2 and are labeled as s1 to s12. Position angles (PAs) for these observations were +25° (s2, s12), +60° (s1, s11), +56° (s3–s9), and −30° (s10).

The first observation run was executed on 2013 December 15 using the 4×4 binning mode (0.702 arcsec pix^{-1} plate scale). The spectra were centered at the [O III]λ5007 emission line using a filter ($\Delta\lambda$=50Å) to isolate the 114$^{\rm th}$ order (0.087 Å pix^{-1} spectral scale). Exposure time was 1800 s for each spectrum (slits s2 and s12).

The second series of spectra were acquired on 2014 January 18 in the 2×2 binning mode (0.351 arcsec pix^{-1} plate scale). Observations were made around the Hα emission line using a filter ($\Delta\lambda$=90Å) to isolate the 87$^{\rm th}$ order (0.1 Å pix^{-1} spectral scale). Exposure time was set to 1800 s. Three slit positions were located to pass through the bright [N II]λ6584 knots as well as the arc-like features avoiding the central star to prevent saturation of the spectra (s1, s10, and s11). Furthermore, slit s10 pass through the major axis and was observed in Hα and [O III]λ5007 spectral ranges, but with a spectral scale of 0.043 Å pix^{-1} and exposure time of 1200 s.

Finally, the third series of spectra was observed on 2014 January 20 with the same technical configuration as the December run. Exposure times were 300 s with the exception of s9 that was 600 s. Seeing was around 1.5 arcsec during the observations (s3 to s9).

Data were processed using standard techniques for long-slit spectroscopy of IRAF. The spectra were wavelength-calibrated with a Th-Ar arc lamp to an accuracy of ±1 km s^{-1}. The FWHM of the arc lamp emission lines was measured to be $\simeq 12\ \pm1$ km s^{-1}.

3 RESULTS

In the following two subsections we present our main results separated in the inner and outer structures, with regard to the two shells and the halo. We also estimated the distance to NGC 3242.

3.1 Inner structures

As can be seen in our direct imaging study, some of the structural components of NGC 3242 appear slightly different according to the wavelength observed (Fig. 1). We detected the two concentric elliptical components: the limb brightening inner shell (28×20 arcsec) surrounded by a diffuse outer shell (46×40 arcsec), structures previously reported by Hromov & Kohomek (1968), in which the major axis are located toward the PA=−40°.

Besides the inner and outer shells, further small structural components were resolved and, as mentioned before, were detected in different wavelengths. These structures are labeled in Fig. 1.

About kinematics, Figure 3 shows Position-Velocity (PV) maps corresponding to the slits s3 to s10, whereas those from s1, s11, and s10 are presented in Figure 4. The radial velocity presented hereby is relative to the systemic velocity $V_{\rm LSR} = -6.6\pm1$ km s^{-1}

[1] The Observatorio Astronómico Nacional (OAN-SPM) is located at the Sierra de San Pedro Mártir, Baja California, and is operated by the Instituto de Astronomía of the Universidad Nacional Autónoma de México (UNAM).

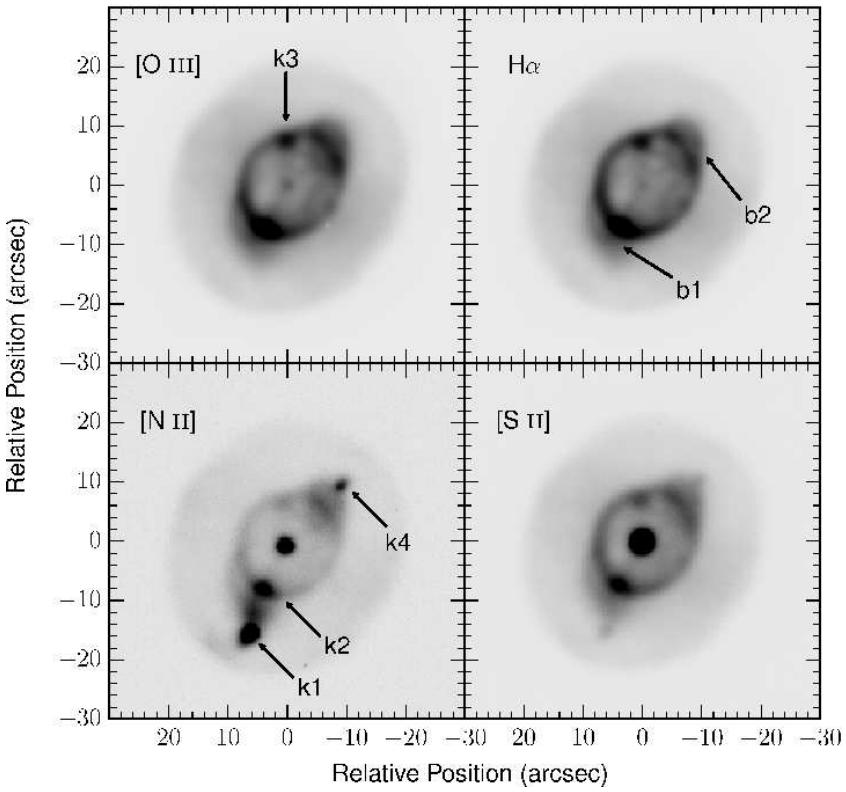

Figure 1. NGC 3242 as seen in (a) H$\alpha\lambda$6563Å, (b) [O III]λ5007Å, (c) [N II]λ6584Å, and (d) [S II]λ6724Å. Arbitrary contrast scales were set to enhance the different features seen in the nebula. North is up and East is left in all the images.

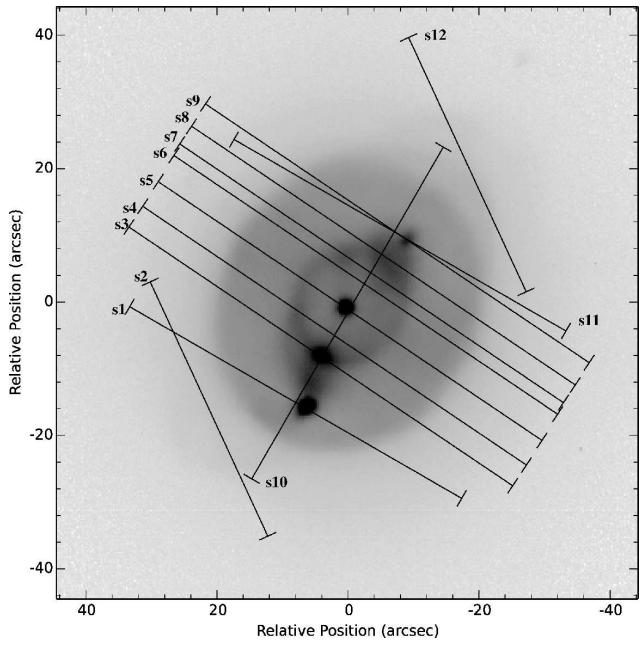

Figure 2. Slits position observed and superimposed in the [O III] + [N II] composite image with arbitrary contrast chosen to enhance the different features present in the nebula. PAs=+25°(s2, s12), +60°(s1,s11), +56°(s3–s9), and –30° (s10).

($V_{\rm Hel} = +1 \pm 1\,{\rm km\,s^{-1}}$) obtained from s10 and which is in good agreement with the value of $\simeq -7.6 \pm 1\,{\rm km\,s^{-1}}$ obtained by Rodríguez et al. (2010). A well-defined velocity ellipsoid dominates the velocity pattern measured, however, distortions corresponding to the inner structures are present and enhanced in our PV diagrams by contours. The measured expansion velocity of the inner shell is 23 $\pm$1 km s^{-1} and is consistent with the value obtained by Balick (1987). As for the outer shell, we have estimated an expansion velocity of $\simeq 13 \pm 1\,{\rm km\,s^{-1}}$ by considering the deprojected separation of two Gaussian components fitted to a line profile from s6 (less deformed velocity ellipsoid), taken at 14 arcsec from the central star in order to avoid confusion from the inner shell. Our value is a typical for this type of outer shell.

Table 1 resumes the main parameters of structures labeled in Fig. 1. Column 1 shows the label of each microstructure (k, for knot, b, for blob). Columns 2 and 3 correspond to the slit and filter used to measure the velocity. Column 4 and 5 indicate the angular distance from the central star, as well as the PA, measured from north to east, for each structure. The radial velocity relative to the systemic velocity is presented in column 6. In the case of the b1 and b2, which also present an expansion, the values in the table represent position and velocity of the center of each blob. unnecessary

In general our results are consistent with previous works in literature.

From Fig. 3 we have also been able to measure the expansion velocity of **b1** and **b2** (see slits s3 and s8, respectively) and the values obtained were 21$\pm$1 km s^{-1} and 16$\pm$1 km s^{-1}, respectively. These values were calculated by fitting a double-peaked Gaussian profile to the spectral lines corresponding to each bubble and considering the contamination of the emission of the inner shell.

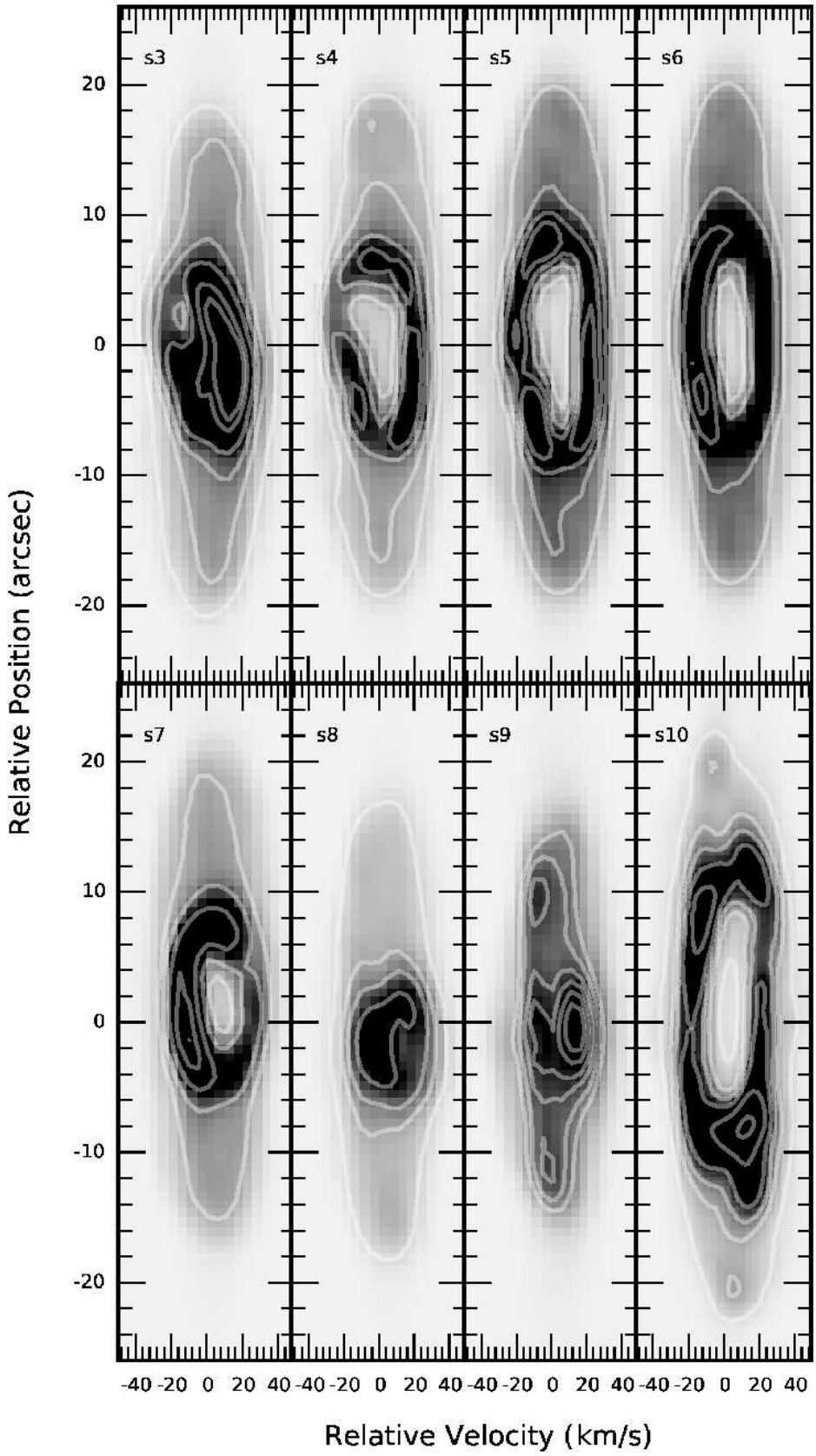

Figure 3. Position-Velocity (PV) maps of the [O III] emission line corresponding to the s3 – s6 (upper panel) and s7 – s10 (lower panel). NE is up in all the panels, except s10, in which NW is up.

Name	Slit	Filter	Distance (arcsec)	PA (°)	$V_{\rm rel}$ (km s^{-1})
k1	s1	[N II]	16	+158	+22±1
k2	s3,s10	[O III], [N II]	9.5	+152	+14
k3	s7	[O III]	7.5	+4	+2.3
k4a	s11	[N II]	14	−40	−28
k4b	s11	[N II]	14	−40	+13
b1	s3	[O III]	8.7	+140	−13
b2	s8	[O III]	8.7	−40	+11

Table 1. Small structures properties of NGC 3242.

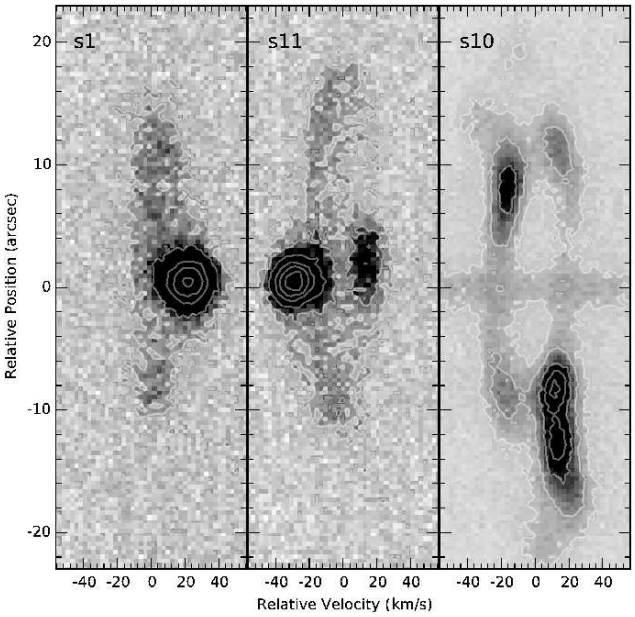

Figure 4. Position-Velocity maps in [N II]. Labels correspond to slit position shown in Fig. 2: s1 (left), s11 (middle) and s10 (right). Position axis is reference to the peak of emission (s1 and s11) and to the central star (s10). NE is up in the panels left and center, whereas NW is up in the right panel.

3.2 Outer structures

In order to enhance the outermost morphological components of NGC 3242, those located in the halo, we applied the widely used unsharp masking technique to the [O III] image (Fig. 5). Despite the inner and outer shells, as well as the features **k2**, **k3**, **b1**, **b2**, dominate the emission of this PN, at least three arcs (**a1**, **a2** and **a3**) are detected beyond the concentric shells. Furthermore, it is remarkable the presence of two pairs of features aligned once more towards NW–SE: **bh1**, **bh2**, **bh3**, **bh4**. These features were previously detected by Blanco Cárdenas (2006) and Phillips et al. (2009). Henceforward, we will refer to these four features as "disruptions" of the halo.

The kinematics of the disruptions were investigated in the PV diagrams of the Figure 6, that is, in the slits s2 and s12. These structures appear like loops in the PV maps. Radial velocity of the central point of each structure, relative to the systemic velocity of the nebula, are shown in Table 2, as well as the expansion velocity ($V_{\rm exp}$) on each case. For each structure, radial velocities are estimated from the center of the loop (mean velocity of the splitting), whereas expansion velocities are estimated as the half of the maximum of each loop (line splitting) in the velocity axis.

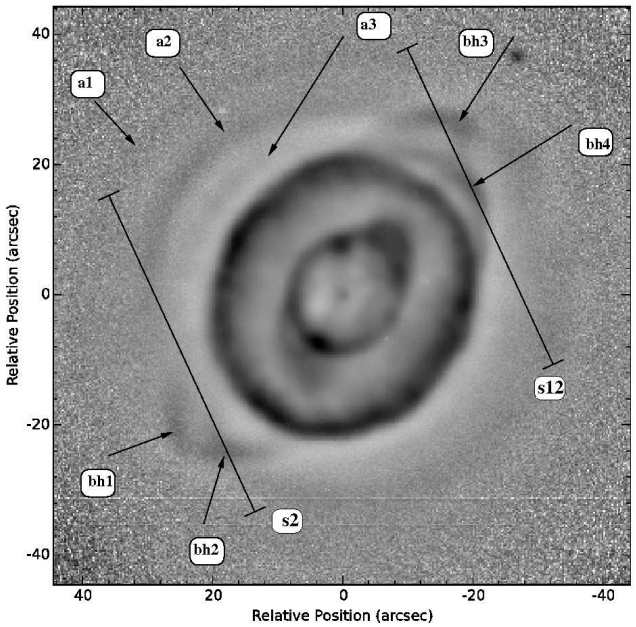

Figure 5. Unsharp-masking logarithmic image in [O III] of NGC 3242. Main morphological features are labeled.

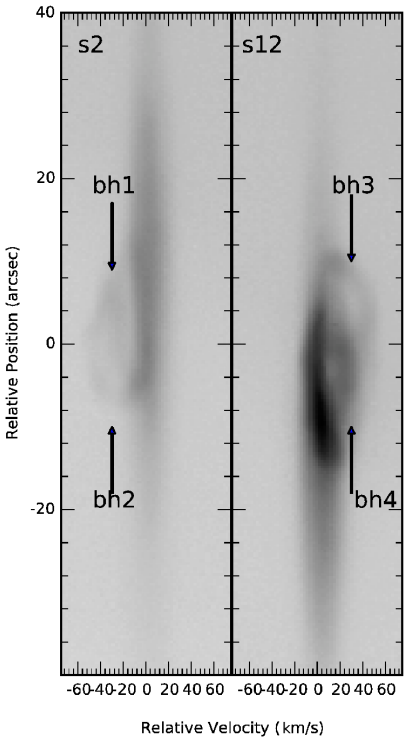

Figure 6. Position-Velocity (PV) maps of the [O III] emission line corresponding to the s2 (left), and s12 (right) slit positions. NE is up in both panels.

3.3 Distance to NGC 3242

Trigonometric parallax for NGC 3242 was early determined by Jenkins (1952), who estimated a value of 30 ± 15 mas. Such value lead to an unreal determination of distance for this nebula. Subsequently, Cahn, Kaler & Stanghellini (1992) reported a distance of 1.08 kpc by means of statistical methods. Using VLA data and an

Structure	$V_{\rm rel}$ (km s^{-1})	$V_{\rm exp}$ (km s^{-1})
bh1	-19 ± 1	11 ± 1
bh2	-29	5
bh3	+29	5
bh4	+13	12

Table 2. Outer structures properties of NGC 3242.

expansion parallax method, Hajian, Terzian, & Bignell (1995) determined a distance to NGC 3242 of 420 ± 160 pc. In this case, data time lapse was around 6 years. A correction to the parallax method was calculated by Mellema (2004), lead to a corrected distance of 550 ± 230 pc to NGC 3242.

In this work, we have estimated a new value for the distance to NGC 3242 using HST imaging from two different epochs, as well as the equatorial expansion velocity described in the Section 3.2 and the SHAPE model presented in Section 4.1.

We got the [OIII] (F502N, $\lambda_{\rm c}=5012$Å, $\Delta\lambda=27$Å) HST images from the MAST archives (programs 6117 [1996] and 11122 [2008], P. I. Bruce Balick). Measurements of the equatorial size along the minor axis of each image (PA=+50°) were performed with the task *splot* of IRAF, co-adding 10 rows to enhance the signal-to-noise ratio. Borders of both sides were de-blended and the extreme components were used to determine the diameters on each image. A difference of 3.44 pixels in diameter (1.72 in radius) was measured. The two different epochs images, as well as the image of the difference, supporting the real nature of the expansion, are presented in Figure 7.

We have determined the distance to NGC 3242 considering a constant velocity and using the following equation, which includes physical units transformation.

$$\left[\frac{r}{\rm pc}\right] = 4.22\left(\frac{\left[\frac{v_{\rm exp}}{\rm km\,s^{-1}}\right]\left[\frac{t}{\rm yr}\right]}{\left[\frac{s}{\rm pixels}\right]}\right)$$

Using the expansion velocity of 23 ± 1 km s^{-1}, the time lapsed as 11.7 ± 0.04 yrs and the 1.72 ± 0.5 pixels from the last paragraph, we have estimate a distance of 660 ± 100 pc, which is in agreement with the determinations of Hajian, Terzian, & Bignell (1995) and even better when comparing with the corrected value from Mellema (2004). It is clear that the uncertainty of the radius dominates the error of this calculation.

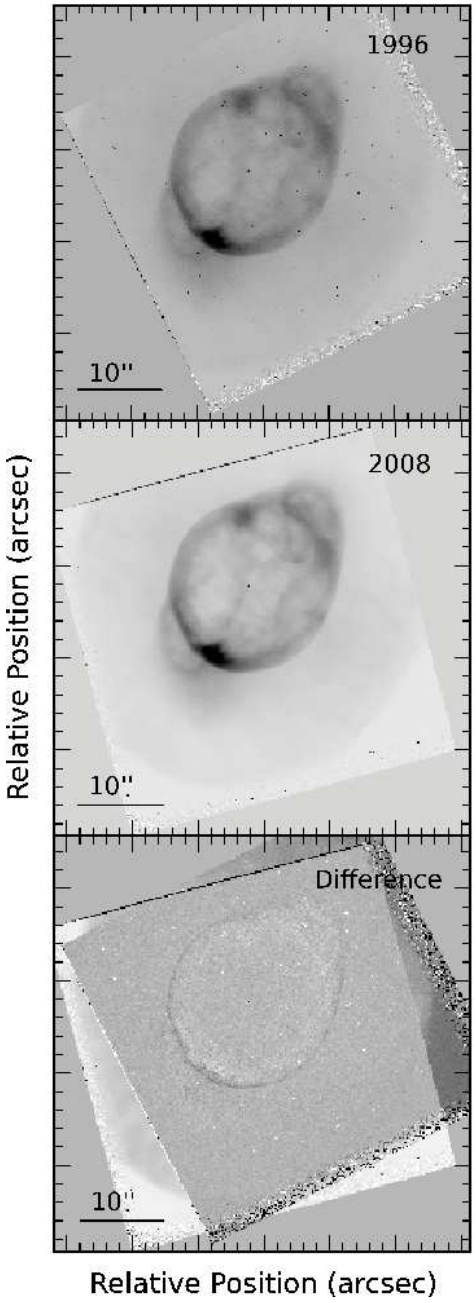

Figure 7. [O III] (F502N) HST images from the MAST archives: programs 6117 [1996] (Top) and 11122 [2008] (middle). The bottom image is the difference of the two HST images.

4 DISCUSSION

4.1 The morpho-kinematic structure of NGC 3242

As described above (Sec. 3.1), our analysis of the high-resolution images indicates that NGC 3242 is a morphologically rich PN with ansae-like features, that resemble bubbles, and knots inside its main structure (Fig. 1). In a first attempt to study the morphology and kinematics of NGC 3242, we have constructed a geometrical model using the interactive software SHAPE (Steffen et al. 2011), a computational tool for morpho-kinematic modeling and reconstruction of astrophysical objects. The internal library of SHAPE includes basic structures such as spheres, cylinders, and torii, which can be modified by applying different parameters and/or functions ('modifiers'). Physical parameters, such as density and velocity, can be assigned to the structures either as an analytical function or interactively. Several recent papers have used SHAPE to get the structure of PNe (e.g., Miszalski et al. 2011; Ramos-Larios et al. 2012; Vázquez 2012; Danehkar & Parker 2015). In our particular case, we obtain a final nebula model that fits the main structure of NGC 3242 for both imaging and spectroscopy (Fig. 8).

We find that NGC 3242 can be modeled as a double-shell elliptical structure. Further, we have been able to calculate the de-projected expansion velocities and radius for the inner shell as well, resulting in values of $R_{\rm eq}=0.03\pm0.004$ pc, $V_{\rm eq}=23$ km s^{-1}, $R_{\rm pol}=0.038\pm0.005$ pc, and $V_{\rm pol}=25.5$ km s^{-1}, whereas the outer shell has an expansion de-projected velocities and radius of $R_{\rm eq}=0.06\pm0.008$ pc, $V_{\rm eq}=10$ km s^{-1}, $R_{\rm pol}=0.074\pm0.01$ pc, and $V_{\rm pol}=13$ km s^{-1} (where eq=equatorial and pol=pole of the

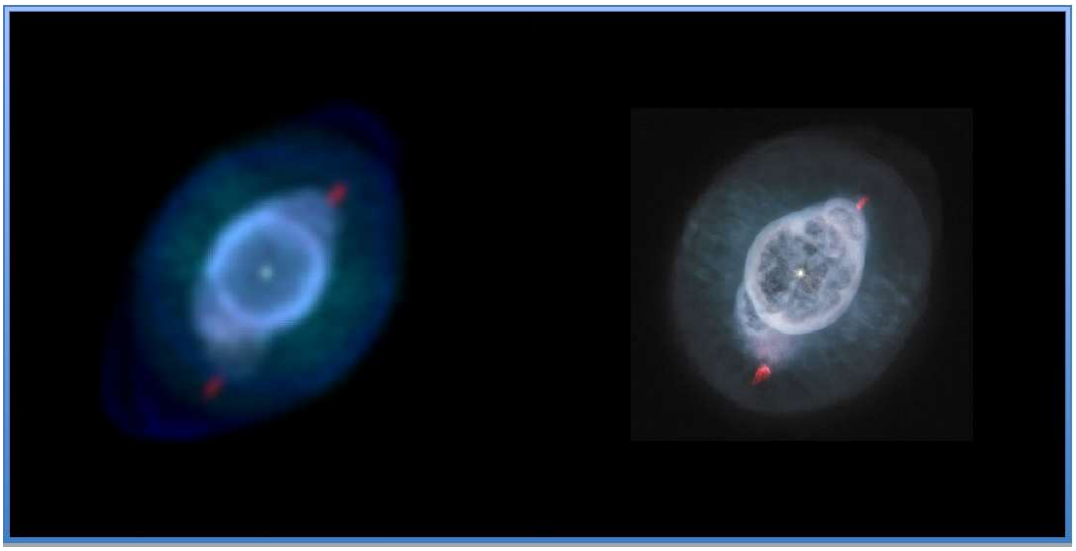

Figure 8. Comparison of the 3D model obtained from SHAPE (left) and the HST image (right).

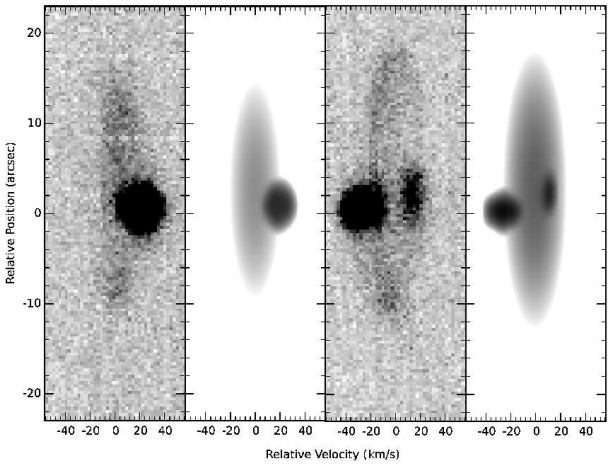

Figure 9. Observed PV-map of the [N II] line for s1 and s11, and the corresponding SHAPE synthetic PV-maps. NE is up in all the panels.

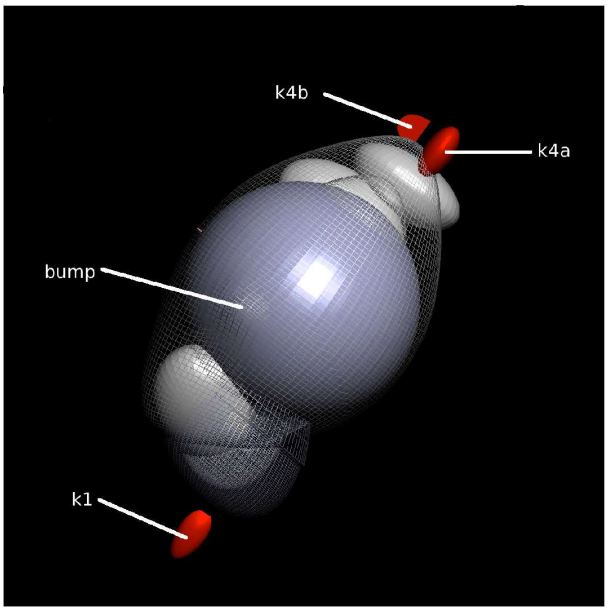

Figure 10. SHAPE model of the inner structures. Knots and bump are highlighted.

ellipse). These values were calculated with observational data presented in Sec. 3 and assuming homologous velocity expansion ($V \propto r$). With the estimation of the distance using the expansion parallax mentioned in section 3.3, we have been able to calculate the kinematical age of the shells resulting in 1400 ± 350 yr and 5400 ± 1300 yr for the inner and outer shells, respectively.

In Table 3 we present properties, such as the de-projected velocities, inclinations, and kinematical ages, derived for the small-scale features described in the results and modeled using SHAPE. In our model of NGC 3242, we used an ellipsoid to generate the feature **k1** presented in the Figure 9. For **k4**, we used a pair of ellipsoids in the model to represent the **k4a** and **k4b** features detected in the s11 PV (see Figure 10). The velocities and the properties of **k1** and **k4a**, previously classified as low ionisation structures (LIS, Gonçalves, Corradi, & Mampaso 2001) and also fast, low ionisation emission regions (FLIERs, Balick et al. 1998), suggest a jet nature for these two structures ($|\vec{v}|$=117 km s^{-1} and $|\vec{v}|$=140 km s^{-1}, respectively), whereas the elongated appearance observed and modelled for **k4b**, as well as its high de-projected velocity ($|\vec{v}|$=121 km s^{-1}), point to the idea of this feature being originated through a collision of the jet **k4a** with the inner shell of NGC 3242, or other disruptive mechanism , but further detailed study will be needed to get insights about the nature of this structure.

It is important to make clear that we have no hard restrictions to choose the inclination angles for the collimated structures. We made our best assumption given our data and model, as well as rational inferences, but we are aware that other angles are possible.

On the other hand, a remarkable feature, seen as a deformation of the bright ellipse of the inner shell, located at $\simeq 3''$from the middle, is clearly noted in the PV of s4. This feature cannot be easily identified in the images, but we can find its location by comparing PV maps with images. The corresponding location appears as a less bright region in the high resolution image of HST (Fig. 8, right). We have interpreted and modelled this feature as a kind

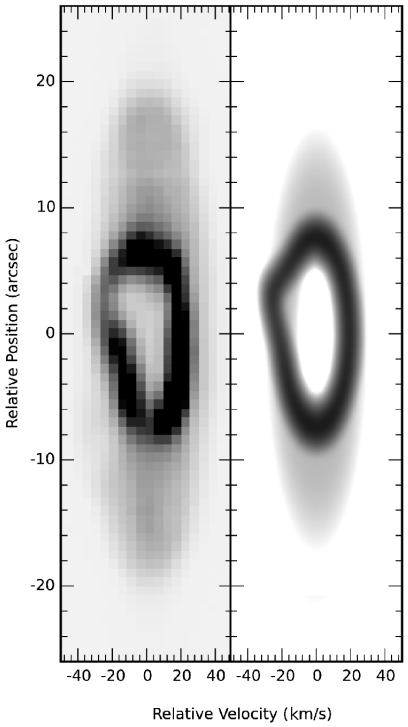

Figure 11. Observed PV-map of the [O III] line at s4 and the corresponding SHAPE synthetic PV-map. NE is up in both panels.

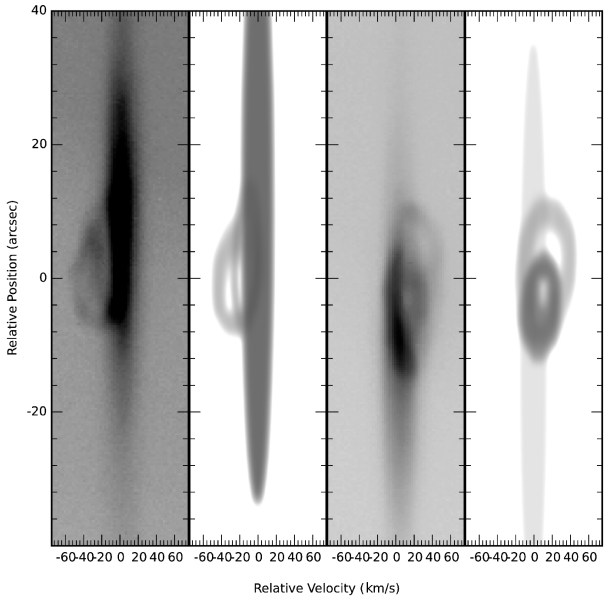

Figure 12. Observed PV-map of the [O III] line for s2 and s12, and their corresponding SHAPE synthetic PV-maps. NE is up in all the panels.

of protrusion, blowing out from the nucleus of the nebula, and deforming the velocity ellipse of the shell. We have used the modifier "bump" in SHAPE to model this protrusion with a Gaussian density profile to enhance it (Fig. 10) to reproduce the deformation (Fig. 11). Possibly, this could be the youngest collimated ejection of the nebula, however the estimate of its kinematical age (1400 yr) is slightly lower than the age of the inner shell. This could be a matter

Name	r (arcsec)	$V_{\rm rel}$ (km s^{-1})	$\lvert\vec{V}\rvert$ (km s^{-1})	PA (°)	i (°)	$\tau_{\rm k}$ (yr)
k1	21	+22	117	158	100	580±120
k4a*	17	−28	140	−43	78	390±100
k4b*	17	+13	121	−43	96	450±100
Bump	14	−23	28	124	17	1600±400
bh1	37	−19	52	131	65	2280±450
bh2	32	−29	130	143	75	800±200
bh3	30	+29	140	−33	102	690±150
bh4	26	+13	83	−50	101	1000±250

* k4a correspond to the blueshift knot and k4b to the redshift knot in the spectra s11.

Table 3. De-projected velocities, inclinations respect to the plane of the sky, and kinematical ages obtained from the main structures detected. The kinematical ages where determined using the distance calculated in the Section 3.3 as well as the de-projected velocities and radius obtained with the model.

of age and/or inclination angle uncertainties, but also could indicate a deceleration of this outflow when interacting with the inner shell.

To model the disruptions in the halo seen in Fig. 5, we used two pair of ellipsoids with a Gaussian density profile for each bubble, reproducing well these disruptions. The radial velocities as well as the de-projected velocities calculated for these components are remarkably high (see Table 3), exceeding the 100 km s^{-1}. A comparison between spectra and model of the disruptions is shown in Fig. 12.

At first, the velocities and the spatial distribution of the polar structures of NGC 3242, the inner knots, whose properties are in agreement with a FLIER nature, as well as the bubbles located between the double-shell structure and the disruptions in the halo, suggest a common origin. That is, the small-scale inner FLIERs and bubbles have compressed and pushed the gas, reaching the halo and thus forming the disruptions observed on these outermost regions. However, the kinematical ages estimated point to separated events, being the inner structures younger than the ones detected on the halo. In summary, the velocities and kinematical ages of the FLIERs, bubbles, and disruptions suggest the presence of a mechanism that triggers episodic ejections in this PN in association with rotation of the collimating engine of NGC 3242 (e.g. NGC 6543, Miranda & Solf 1992).

4.2 The formation of NGC 3242

We support the scenario in which the inner shell of NGC 3242 was formed through the shock front produced by the interaction of the stellar winds (Kwok, Purton & Fitzgerald 1978), whereas the outer shell can be interpreted as the AGB envelope remnant, considering the kinematics hereby reported as well as the physical conditions reported in previous studies (Meaburn, López, & Noriega-Crespo 2000; Ramos-Larios & Phillips 2009; Ruiz et al. 2011; Monteiro et al. 2013). As for the kinematics of the inner FLIERs, bubbles, and disruptions in the halo, we have analysed them with unprecedented detail. The preference direction, towards NW–SE (Fig. 2), of all these morphological components may be related with some mechanism able to collimate such structures, likely in different events (e.g., Miranda & Solf 1992; López, Vázquez, & Rodríguez 1995; Palmer et al. 1996; Vázquez et al. 2008; Rubio et al. 2015).

As stated before, from the morphological and kinematical data, we have analysed for the first time the morpho-kinematic structure of the four disruptions in the halo of NGC 3242 (**bh1**,

bh2, **bh3**, **bh4**). The small difference between the radial and the de-projected velocities of **bh1** with respect to **bh4**, as well as **bh2** and **bh3**, in addition to their kinematical ages suggest that these four structures were probably formed by the same phenomenon. This occurs when a collimated outflow passed through the outer shell breaking or pushing this shell as a result of the hight velocity of the jet. As a consequence, this leaves the diffuse disruptions as remnant of this collimated ejection (differences could be originated by inhomogeneous medium). On the other hand, the inner FLIERs and bubbles were likely formed by a later ejection, being the last morphological structures formed in this PN.

In the case of the southern FLIER **k1**, noticeably orientated towards the south, not in the SE direction like the rest of the structures, it is possible that **k1** has followed this trajectory due a deflection originated by higher density zones along the inner shell of NGC 3242. In this context, the value for the N_e reported by Ruiz et al. (2006) for this shell is $\simeq 2200\,\mathrm{cm}^{-3}$, however, the zones towards **k1** and **k4**, including the knot **k2**, have higher electronic densities, up to $4000\,\mathrm{cm}^{-1}$ or greater, accordingly to the analysis of the physical conditions carried out by Monteiro et al. (2013). Besides the velocities hereby reported and the densities measured in previous studies, the jet nature of the FLIERs **k1** and **k4** is favored considering their emission in low-excitation emission lines, a well known cooling mechanism of shocked gas. The knots **k2** and **k3**, emitting also in high-excitation lines, may be produced by shocked material as well, although, the values for the electronic temperature in these zones (T_e=12,000 K) reported by Monteiro et al. (2013) are not considerably higher than the values obtained for the rest of the nebula (10,000 K$>$ T_e $>$15,000 K). On the other hand, there is clear evidence of filamentary structures related with thermal dust and gas beyond the outer shell and the halo of this PN, indicating that NGC 3242 was born in a clumpy environment (Ramos-Larios & Phillips 2009), interacting with the surrounding ISM, likely affecting the formation of some structures due to the presence of this dusty material.

5 CONCLUSIONS

From the kinematic study we derived a systemic velocity for NGC 3242 of $V_\mathrm{LSR} = -6.6 \pm 1\,\mathrm{km\,s}^{-1}$. We also reassert that NGC 3242 is a multiple-shell PN. The inner shell has an expansion velocity of $\simeq$23 km s^{-1}, meanwhile, the outer shell has an expansion velocity of $\simeq$13 km s^{-1}. Further, beyond its multiple shell structure, we analysed the radial velocity of the disruptions in the halo located toward NW–SE along major axis of the PN, whereas the radial velocities are 29 km s^{-1} and 13 km s^{-1} and, -19 km s^{-1} and -29 km s^{-1}, respectively. Employing the expansion parallax method and using HST imaging from two different epochs, we have been able to estimated a new distance value of to the nebula of $d = 660 \pm 100$ pc.

A detailed morpho-kinematic model was built using the computational software SHAPE fitting our data and improving our interpretation of the structure of NGC 3242. Our model is consistent with an outer shell with a semi-major axis of 0.072 pc (V_pol=13 km s^{-1}), possibly disrupted by collimated outflows passing through it, and an inner shell with semi-major axis of 0.037 pc (V_pol=25.5 km s^{-1}), and likely deformed by jets with a FLIER nature. According to our model, the disruptions in the halo have inclination angles of $i = 65^\circ$ and $i = 75^\circ$ toward SE, and $i = 101^\circ$ and $i = 102^\circ$ toward NW, where the de-projected velocities are 52 km s^{-1}, 130 km s^{-1}, 83 km s^{-1}, and 140 km s^{-1}, respectively. Moreover, the jets in the inner shell have inclination angles of $i = 100^\circ$ and PA=+160°and, $i = 78^\circ$ and PA=-40°, whereas the de-projected velocities are 117 km s^{-1} and 140 km s^{-1}, respectively. The preferential direction, towards NW–SE of all these morphological components may be related with some mechanism able to collimate and eject such structures episodically.

In our scenario, the outer shell is the oldest structure (5400 yr), then, some material was ejected and the first disruptions appear (**bh1** and **bh4**), protruding in the shell and partially in the halo. After that, the second disruptions were ejected (possibly at a higher velocity, **bh2** and **bh3**). The inner shell was ejected after the **bh**s, and then the "bump". Finally, the features **k** were ejected and they interacted with the inner shell. All these results, as well those derived in previous studies, suggest that all the morphological components of NGC 3242 apparently were originated in a clumpy medium. Inconsistencies in ages of the inner shell and the bump, as well as **bh2**, **bh3**, and **bh4**, are small enough to be explain with age and inclination angle uncertainties.

ACKNOWLEDGMENTS

We are grateful to the staff of OAN-SPM, specially to Mr. Gustavo Melgoza-Kennedy, our telescope operator, for his assistantship during observations. This paper has been supported by Mexican grant IN107914 (PAPIIT- DGAPA-UNAM). SZ acknowledges support from the UNAM-ITE collaboration agreement 1500-479-3-V-04. SA acknowledges support from the UNAM-UANL collaboration agreement. This research has made use of the SIMBAD database, operated at CDS, Strasbourg, France. IRAF is distributed by the National Optical Astronomy Observatories, which are operated by the Association of Universities for Research in Astronomy, Inc., under cooperative agreement with the National Science Foundation. MAGM acknowledges CONACYT for his graduate scholarship. Authors are deeply grateful to Prof. Michael Richer for a kind and careful revision of the manuscript. Authors are grateful to the anonymous referee whose comments were truly valuable and helped to improve this article.

REFERENCES

Acker A., Marcout J., Ochsenbein F., Stenholm B., Tylenda R., 1992, Strasbourg ESO Catalogue of Galactic Planetary Nebulae. Part 1; Part 2. European Southern Observatory, Garching
Balick B., Alexander J., Hajian A. R., Terzian Y., Perinotto M., Patriarchi P., 1998, AJ, 116, 360
Balick B., Frank A., 2002, ARA&A, 40, 439
Balick, B. 1987, AJ, 94, 671
Blanco Cárdenas, M. W., 2006, BSc thesis, Facultad de Ciencias, Universidad Autónoma de Baja California (México)
Cahn J. H., Kaler J. B., Stanghellini L., 1992, A&A, 94, 399
Corradi R. L. M., Schönberner D., Steffen M., Perinotto M., 2003, MNRAS, 340, 417
Corradi R. L. M., Sánchez-Blázquez P., Mellema G., Giammanco C., Schwarz H. E., 2004, A&A, 417, 637
Danehkar A., Parker, Q. A., 2015, MNRAS, 449, L56
Gonçalves D. R., Corradi R. L. M., Mampaso A., 2001, ApJ, 547, 302
Hajian A. R., Terzian Y., Bignell C., 1995, AJ, 109, 2600
Hromov G. S., Kohomek L., 1968, BAICz, 19, 1

Jenkins, L. F. 1952, General Catalogue of Trigonometric Stellar Parallaxes (New Haven, CT, Yale University Observatory)
Kwok S., Purton C. R., FitzGerald P. M., 1978, ApJ, 219, L125
López J. A., Vázquez R., Rodríguez L. F., 1995, ApJ, 455, L63
Manchado A., Stanghellini L., Guerrero M. A., 1996b, ApJ, 466, 95
Meaburn J., López J. A., Gutiérrez L., Quirós F., Murillo J. M., Valdez J., Pedrayes M., 2003, RevMexAA, 39, 185
Meaburn J., López J. A., Noriega-Crespo A., 2000, ApJS, 128, 321
Mellema G., 2004, A&A, 416, 623
Miranda L. F., Solf J., 1992, A&A, 260, 397
Miszalski B., Corradi R. L. M., Boffin H. M. J., Jones D., Sabin L., Santander-García M., Rodríguez-Gil P., Rubio-Díez M. M., 2011, MNRAS, 413, 1264
Monreal-Ibero A., Roth M. M., Schönberner D., Steffen M., Böhm P., 2005, ApJ, 628, L139
Monteiro H., Gonçalves D. R., Leal-Ferreira M. L., Corradi R. L. M., 2013, A&A, 560, AA102
Palmer J. W., Lopez J. A., Meaburn J., Lloyd H. M., 1996, A&A, 307, 225
Phillips J. P., Ramos-Larios G., Schröder K.-P., Contreras J. L. V., 2009, MNRAS, 399, 1126
Ramos-Larios G., Phillips J. P., 2009, MNRAS, 400, 575
Ramos-Larios G., Vázquez R., Guerrero M. A., Olguín L., Marquez-Lugo R. A., Bravo-Alfaro H., 2012, MNRAS, 423, 3753
Rodríguez L. F., Gómez Y., López J. A., García-Díaz M. T., Clark D. M., 2010, RMxAA, 46, 29
Rubio G., Vázquez R., Ramos-Larios G., Guerrero M. A., Olguín L., Guillén P. F., Mata H., 2015, MNRAS, 446, 1931
Ruiz N., Guerrero M. A., Chu Y.-H., Gruendl R. A., Kwitter K. B., Meixner M., 2006, IAUS, 234, 497
Ruiz N., Guerrero M. A., Chu Y.-H., Gruendl R. A., 2011, AJ, 142, 91
Schwarz H. E., Corradi R. L. M., Melnick J., 1992, A&ASS, 96, 23
Steffen W., Koning N., Wenger S., Morisset C., Magnor M., 2011, ITVCG, 17, 454
Steffen M., Schönberner D., 2003, IAUS, 209, 439
Terzian Y., 1997, IAUS, 180, 29
Vázquez R., 2012, ApJ, 751, 116
Vázquez R., Miranda L. F., Olguín L., Ayala S., Torrelles J. M., Contreras M. E., Guillén P. F., 2008, A&A, 481, 107